1521-0103/344/3/655–664$25.00
THE JOURNAL OF PHARMACOLOGY AND EXPERIMENTAL THERAPEUTICS

http://dx.doi.org/10.1124/jpet.112.201475
J Pharmacol Exp Ther 344:655–664, March 2013

Mechanisms Limiting Distribution of the Threonine-Protein Kinase B-RaF^{V600E} Inhibitor Dabrafenib to the Brain: Implications for the Treatment of Melanoma Brain Metastases[S]

Rajendar K. Mittapalli, Shruthi Vaidhyanathan, Arkadiusz Z. Dudek, and William F. Elmquist

Department of Pharmaceutics, Brain-Barriers Research Center (R.K.M., S.V., W.F.E.), and Divison of Hematology, Oncology and Transplantation, Department of Medicine (A.Z.D.), University of Minnesota, Minneapolis, Minnesota

Received October 29, 2012; accepted December 14, 2012

ABSTRACT

Brain metastases are a common cause of death in stage IV metastatic melanoma. Dabrafenib is a BRAF (gene encoding serine/threonine-protein kinase B-Raf) inhibitor that has been developed to selectively target the valine 600 to glutamic acid substitution (BRAF^{V600E}), which is commonly found in metastatic melanoma. Clinical trials with dabrafenib have shown encouraging results; however, the central nervous system distribution of dabrafenib remains unknown. Thus, the objective of the current study was to evaluate the brain distribution of dabrafenib in mice, and to see whether active efflux by P-glycoprotein (P-gp) and breast cancer resistance protein (BCRP) restricts its delivery across the blood-brain barrier (BBB). In vitro accumulation studies conducted in Madin-Darby canine kidney II cells indicate that dabrafenib is an avid substrate for both P-gp and BCRP. Directional flux studies revealed greater transport in the basolateral to apical direction with corrected efflux ratios greater than 2 for both P-gp and Bcrp1 transfected cell lines. In vivo, the ratio of area under the concentration-time curve $(AUC)_{brain}$ to AUC_{plasma} (K_p) of dabrafenib after an i.v. dose (2.5 mg/kg) was 0.023, which increased by 18-fold in Mdr1 *a/b*$^{-/-}$*Bcrp1*$^{-/-}$ mice to 0.42. Dabrafenib plasma exposure was ~2-fold greater in Mdr1 *a/b*$^{-/-}$*Bcrp1*$^{-/-}$ mice as compared with wild-type with an oral dose (25 mg/kg); however, the brain distribution was increased by ~10-fold with a resulting K_p of 0.25. Further, compared with vemurafenib, another BRAF^{V600E} inhibitor, dabrafenib showed greater brain penetration with a similar dose. In conclusion, the dabrafenib brain distribution is limited in an intact BBB model, and the data presented herein may have clinical implications in the prevention and treatment of melanoma brain metastases.

Introduction

Melanoma is the most aggressive form of skin cancer, as it accounts for more than 80% of deaths due to skin cancer. The incidence of melanoma has greatly increased over the past decade (Siegel et al., 2011). Extensive data in the literature point to the key role of the mitogen-activated protein kinase (MAPK) pathway in melanoma pathogenesis. The MAPK pathway is involved in regulation of melanoma cell proliferation, growth, and survival. The downstream effectors of this signaling cascade include RAS-RAF-MEK-ERK (McCubrey et al., 2008). BRAF is a commonly mutated protein in melanoma, with ~80% carrying a V600E (BRAF^{V600E}) mutation (Davies et al., 2002). Thus, targeting this pathway represents an attractive therapeutic approach for melanoma.

Until recently, treatment options for melanoma were limited, with no improvement in overall survival rates (Tsao et al., 2004; Garbe et al., 2011). However, in recent years, there has been a tremendous improvement in the treatment of melanoma. Targeting BRAF^{V600E} has proved to be a major advancement in the field of melanoma treatment (Flaherty et al., 2012; Sosman et al., 2012). For example, the recently U.S. Food and Drug Administration (FDA)–approved drug vemurafenib, a BRAF^{V600E} inhibitor, showed remarkable efficacy against peripheral metastases (Chapman et al., 2011). However, brain metastases are prevalent in stage IV

This work was supported in part by the National Institutes of Health National Cancer Institute [Grant CA138437].
dx.doi.org/10.1124/jpet.112.201475.
[S] This article has supplemental material available at jpet.aspetjournals.org.

ABBREVIATIONS: A, apical; AG1478, 4-(3-chloroanilino)-6,7-dimethoxyquinazoline; AUC, area under the concentration-time curve; B, basolateral; BBB, blood-brain barrier; BCRP, breast cancer resistance protein; *Bcrp1*, gene encoding the murine breast cancer resistance protein; B/P, brain to plasma; BRAF, gene encoding serine/threonine-protein kinase B-Raf; CNS, central nervous system; ERK, extracellular signal-regulated kinase; FDA, Food and Drug Administration; f_u, free fraction; $f_{u,brain}$, unbound fraction in brain homogenate; $f_{u,plasma}$, unbound fraction in plasma; FVB, Friend leukemia virus strain B; Ko143, (3S,6S,12aS)-1,2,3,4,6,7,12,12a-octahydro-9-methoxy-6-(2-methylpropyl)-1,4-dioxopyrazino(1',2':1,6) pyrido(3,4-b)indole-3-propanoic acid 1,1-dimethylethyl ester; K_p, ratio of AUC_{brain} to AUC_{plasma}; $K_{p,uu}$, ratio of unbound drug in brain to unbound drug in plasma; LC-MS/MS, liquid chromatography–-tandem mass spectrometry; LY335979 (zosuquidar), (R)-4-[(1aR,6R,10bS)-1,2-difluoro-1,1a,6,10b-tetrahydrodibenzo-(a,e)cyclopropa(c)cycloheptan-6-yl]-α-[(5-quinoloyloxy) methyl]-1-piperazine ethanol, trihydrochloride; MAPK, mitogen-activated protein kinase; MDCKII, Madin-Darby canine kidney II; MDR1, gene encoding the human P-glycoprotein; *Mdr1*, gene encoding the murine P-glycoprotein; MEK, methyl ethyl ketone; P_{app}, apparent permeability; PBS, phosphate-buffered saline; P-gp, p-glycoprotein; WT, wild type.

metastatic melanoma. This situation is alarming because ~50–75% of melanomas metastasize to the brain (Fife et al., 2004), and among those patients who have brain metastases, ~90% succumb to death (Skibber et al., 1996). The efficacy of vemurafenib in brain metastases of melanoma is under clinical investigation. Recent preclinical studies have indicated that vemurafenib distribution is restricted at the blood-brain barrier (BBB) (Durmus et al., 2012; Mittapalli et al., 2012).

Dabrafenib (GSK2118436A; Fig. 1) targets both $BRAF^{V600E}$ and $BRAF^{V600K}$. Dabrafenib showed very encouraging results in a phase 1 dose-escalation study (Falchook et al., 2012; Hauschild et al., 2012). The safety and clinical response of dabrafenib against peripheral metastases is comparable with that of vemurafenib, with an objective response of ~56% (Gibney and Sondak, 2012; Hauschild et al., 2012). Further, ~90% (9 out of 10 patients) of the patients with melanoma brain metastases had a reduction in tumor size (Falchook et al., 2012). However, important questions remain about the effective delivery to all sites of brain metastases, especially to the micrometastases which are situated beyond an intact BBB. In a recent study, using a preclinical model of brain metastases from breast cancer, it was shown that the blood-tumor barrier remains a significant impediment to chemotherapeutic drugs (Lockman et al., 2010). However, to date, there are no data available in terms of drug delivery to brain metastases of melanoma. Further, it was shown that treatment of peripheral disease with targeted therapy increases the incidence of brain metastases (Rochet et al., 2012). A phase 2 clinical trial evaluating the efficacy of dabrafenib in brain metastases of melanoma is underway (Long et al., 2012; http//www.clinicaltrials.gov identifier: NCT01266967). With this perspective, it is imperative to study the brain distribution of dabrafenib to provide a rationale to support clinical trials.

A critical challenge in treating brain metastases, or any neurologic disorder, is the delivery of drugs to the central nervous system (CNS). The BBB, an interface between blood and the brain, helps maintain homeostasis of the CNS, and protects the brain from harmful toxins, metals, and infectious agents (Deeken and Loscher, 2007). Together with capillary endothelial cells and tight junctions, it acts as a physical barrier (Hawkins and Davis, 2005). Further, with the expression of active efflux transporters such as P-glycoprotein (P-gp) and breast cancer resistance protein (BCRP), it acts as a functional barrier (Schinkel and Jonker, 2003). Several anticancer agents have been shown to be substrates for both P-gp and BCRP, and as such, the brain distribution of these molecules is limited because of active efflux at the BBB (de Vries et al., 2007; Polli et al., 2009; Agarwal et al., 2010, 2011; Mittapalli et al., 2012).

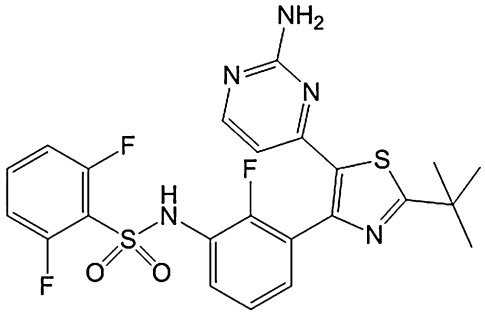

Fig. 1. Chemical structure of dabrafenib (GSK2118436A).

In our previous study, we demonstrated that the brain distribution of vemurafenib is severely restricted at the BBB due to active efflux by both P-gp and BCRP (Mittapalli et al., 2012). Given the highly encouraging clinical results with dabrafenib, the aim of the present study was to evaluate the brain distribution of dabrafenib in mice, with the hope that these preclinical data would help in further improvement of a durable response in melanoma brain metastases patients. Using both in vitro transport studies and in vivo pharmacokinetic studies, we show that dabrafenib is a substrate for both P-gp and Bcrp, and as such, its brain distribution is limited in an intact BBB model. The data presented in this paper have clinical implications in the prevention or treatment of melanoma brain metastases because of concerns that subtherapeutic concentrations in the brain or at sites of micrometastases with an intact BBB would result in limited antitumor activity.

Materials and Methods

Chemicals

Dabrafenib (GSK2118436A) was purchased from ChemieTek (Indianapolis, IN). [^{3}H]-Vinblastine and [^{3}H]-mitoxantrone were purchased from Moravek Biochemicals (La Brea, CA). [^{3}H]-Prazosin was purchased from PerkinElmer Life and Analytical Sciences (Waltham, MA). [^{14}C]-Inulin was purchased from American Radiolabeled Chemicals, Inc. (St. Louis, MO). Ko143 [(3S,6S,12aS)-1,2,3,4,6,7,12,12a-octahydro-9-methoxy-6-(2-methylpropyl)-1,4-dioxopyrazino(1',2':1,6) pyrido(3,4-b)indole-3-propanoic acid 1,1-dimethylethyl ester] was purchased from Tocris Bioscience (Ellisville, MO). Zosuquidar [LY335979, (*R*)-4-([1*aR*, 6*R*,10*bS*]-1,2-difluoro-1,1*a*,6,10*b*-tetrahydrodibenzo-[*a*,*e*] cyclopropa [*c*]cycloheptan-6-yl)-([5-quinoloyloxy] methyl)-1-piperazine ethanol, trihydrochloride] was provided Eli Lilly and Co. (Indianapolis, IN). All other chemicals used were of high-performance liquid chromatography or reagent grade and were obtained from Sigma-Aldrich (St. Louis, MO).

In Vitro Studies

Polarized Madin-Darby canine kidney II (MDCKII) cells were used for all in vitro studies. MDCKII–wild-type (WT) and Bcrp1-transfected (MDCKII-Bcrp1) cells were a gift from Dr. Alfred Schinkel (The Netherlands Cancer Institute, Amsterdam, The Netherlands). MDCKII-WT and gene encoding the human P-glycoprotein (MDR1)-transfected (MDCKII-MDR1) cell lines were provided by Dr. Piet Borst (The Netherlands Cancer Institute). Cells were cultured in Dulbecco's modified Eagle's medium supplemented with 10% (v/v) fetal bovine serum and antibiotics (penicillin, 100 U/ml; streptomycin, 100 μg/ml; and amphotericin B, 250 ng/ml). Cells were grown in 25 ml of tissue culture–treated flasks before seeding for the experiments, and were maintained at 37°C in a humidified incubator with 5% CO_2. The growth media for MDCKII-MDR1 additionally contained 80 ng/ml of colchicine to maintain positive selection pressure of P-gp expression.

In Vitro Cellular Accumulation. Cellular accumulation studies were performed in 12-well polystyrene plates with a seeding density of 2×10^5 cells per well, and the medium was changed every other day until confluent monolayers were formed. The cells were washed two times with warm cell assay buffer (122 mM NaCl, 25 mM $NaHCO_3$, 10 mM glucose, 10 mM HEPES, 3 mM KCl, 2.5 mM $MgSO_4$, 1.8 mM $CaCl_2$, and 0.4 mM K_2HPO_4) on the day of the experiment and

preincubated with cell assay buffer for 30 minutes. The cell assay buffer was aspirated after the preincubation period, and the experiment was initiated by adding 1 ml of 2 μM dabrafenib to each well and further incubated for 60 minutes in an orbital shaker (60 rpm) that was maintained at 37°C. At the end of the 60-minute accumulation, the experiment was ended by aspirating the dabrafenib solution followed by washing twice with ice-cold phosphate-buffered saline (PBS). Cell lysis was accomplished by adding 0.5 ml of 1% Triton-X100 (Sigma-Aldrich). When the inhibitor was present, it was included in both preincubation and the accumulation steps. The concentration of dabrafenib in solubilized cell fractions was analyzed using liquid chromatography–tandem mass spectrometry (LC-MS/MS) as described later, and was normalized to the protein content.

Bcrp and P-gp Inhibition Studies. Inhibition studies were performed using prototypical probe substrates, [^{3}H]-prazosin, or [^{3}H]-mitoxantrone for Bcrp and [^{3}H]-vinblastine for P-gp. The intracellular accumulation of these probe substrates was evaluated in the presence of varying concentrations of dabrafenib ranging from 0.1 to 50 μM. Briefly, the cells were preincubated with increasing concentrations of dabrafenib for 30 minutes. After preincubation, the cells were incubated with radiolabeled probe substrate along with increasing concentrations of dabrafenib for 60 minutes. At the end of the incubation period, the radiolabeled probe substrate was aspirated; cell lysis was accomplished using 1% Triton-X100. The radioactivity in solubilized cell fractions was determined by liquid scintillation counting (LS-6500; Beckman Coulter, Fullerton, CA). The radioactivity in cell fractions was normalized to protein concentrations in each well. The increase in cellular accumulation of probe substrate as compared with control (no treatment with dabrafenib) was measured and reported as a function of dabrafenib concentration.

Directional Flux Studies. The bidirectional transport assays were performed in 12-well Transwell plates (polyester membrane, 0.4-μM pore size, 1.12-cm^2 growth surface area; Corning Inc., Corning, NY). The cells were seeded at a density of 2×10^5 cells per well, and the medium was changed every other day until confluent monolayers were formed. The monolayer tightness was assessed by measurement of transepithelial electrical resistance. In parallel, the cell monolayer integrity was evaluated by analyzing the leakage of [^{14}C]-inulin using the same passage cells seeded on the same day and at the same density.

On the day of the experiment, the cell monolayers were washed with prewarmed cell assay buffer and preincubated for 30 minutes, after which the experiment was initiated by adding 5 μM dabrafenib solution in cell assay buffer to the donor compartment. Samples (100 μl) were collected from the receiver compartment at 60, 120, and 180 minutes and replaced immediately with drug-free cell assay buffer. In addition, at the beginning of the experiment, 100 μl of sample was collected from the donor compartment and replaced with 100 μl of drug solution. The Transwell assay plates were incubated in an orbital shaker (60 rpm) maintained at 37°C for the duration of the experiment, except for the brief sampling times. In the inhibition experiments, either 0.2 μM Ko143 (selective Bcrp inhibitor) or 1 μM zosuquidar (selective P-gp inhibitor) was added to both apical (A) and basolateral (B) compartments. Dabrafenib concentration was measured by LC-MS/MS. The apparent permeability (P_{app}), in the A-to-B and B-to-A directions, was calculated as follows: $P_{app} = (dQ/dt)\,(1/A \times C_0)$, where dQ/dt is the slope obtained from the initial linear range from the amount transported versus time graph, A is the area of the Transwell membrane, and C_0 is the initial donor concentration. The efflux ratio and the corrected efflux ratio were calculated as follows: efflux ratio = $[P_{app}\,(B \rightarrow A) / P_{app}\,(A \rightarrow B)]$ and corrected efflux ratio = (efflux ratio in transfected cells) / (efflux ratio in wild-type cells), where A→B represents permeability in the apical to basolateral direction and B→A represents permeability in the basolateral to apical direction.

Equilibrium Dialysis Experiments. Unbound fractions in mouse plasma and brain homogenates were determined using equilibrium dialysis cassettes (Fisher Scientific, Waltham, MA; Acrylic, 1 ml) as described by Kalvass et al. (2007). For initial pilot studies, commercial mouse plasma (Valley Biomedical, Winchester, VA) and pooled brain homogenates from wild-type and knockout mice were used to determine the time to reach equilibrium (Supplemental Fig. 3). Once the time to reach equilibrium was determined, the free fraction experiments were performed in plasma and brains isolated freshly from either wild-type or *Mdr1a/b*$^{-/-}$*Bcrp1*$^{-/-}$ mice. Spectra/por dialysis membranes (molecular weight cutoff: 12–14 kDa; Spectrum Laboratories, Inc., Rancho Dominguez, CA) were equilibrated in high-performance liquid chromatography water for 30 minutes followed by 30 minutes in extracellular fluid buffer (pH 7.4). Three volumes of ECF buffer was added to the brain tissue and homogenized to attain a uniform homogenate. Dabrafenib was added to plasma and brain homogenate to achieve a final concentration of 2 μM; 1 ml ($n = 3$) was loaded into the equilibrium dialysis cassette and dialyzed against an equal volume of ECF buffer (pH 7.4) in an orbital shaker (200 rpm) maintained at 37°C. Equilibrium was achieved in ~6 hours in both plasma and brain homogenates (Supplemental Fig. 3). At the end of the experiment, matrix (plasma or brain homogenate) and buffer samples were removed from the dialysis cassette, and the concentrations of dabrafenib were measured using LC-MS/MS.

In Vivo Studies

All of the in vivo studies were performed in Friend leukemia virus strain B (FVB; wild-type) and *Mdr1a/b*$^{-/-}$*Bcrp1*$^{-/-}$ (triple knockout) mice of either sex from an FVB genetic background (Taconic Farms, Germantown, NY). All animals were 8–10 weeks old at the time of the experiment. Animals were maintained in a 12-hour light/dark cycle with unlimited access to food and water. All studies were carried out in accordance with the guidelines set by the *Principles of Laboratory Animal Care* (National Institutes of Health, Bethesda, MD) and approved by the Institutional Animal Care and Use Committee of the University of Minnesota.

Plasma and Brain Pharmacokinetics of Dabrafenib after Intravenous and Oral Administration. All dosing formulations of dabrafenib were prepared on the day of the experiment. Dabrafenib dosing formulations were prepared either as a solution in a vehicle containing dimethylsulfoxide, propylene glycol, and water (40:40:20; for i.v. dosing studies) or as a stable suspension in 1% carboxymethyl cellulose (for oral dosing studies).

In the first study, an i.v. dose of 2.5 mg/kg was administered to FVB wild-type and *Mdr1a/b*$^{-/-}$*Bcrp1*$^{-/-}$ mice via the tail vein. Blood and brain samples were collected 5, 15, 30, 60, and 120 minutes postdose ($n = 4$ at each time point). Animals were euthanized using a CO_2 chamber at the desired time point. Blood was collected by cardiac puncture, and plasma was harvested. The whole brain was removed from the skull and washed with ice-cold PBS; superficial meninges were removed by blotting with tissue paper. Plasma and brain specimens were stored at −80°C until further analysis.

In another study, 25 mg/kg of dabrafenib was administered to FVB wild-type and *Mdr1a/b*$^{-/-}$*Bcrp1*$^{-/-}$ mice via oral gavage. Blood and brain samples were harvested at 15, 30, 60, 120, and 240 minutes postdose ($n = 4$ at each time point) as described previously. Brain concentrations were corrected for residual drug in brain vasculature assuming a vascular volume of 1.4% in mouse brain (Dai et al., 2003).

LC-MS/MS Analysis. The concentrations of dabrafenib from all in vitro and in vivo studies were determined using a specific and sensitive LC-MS/MS assay. Brain samples were thawed to room temperature and homogenized with 3 volumes of 5% bovine serum albumin in PBS. An aliquot of sample (cell lysate, cell assay buffer, plasma, or brain homogenate) was spiked with 10 ng of internal standard [AG1478; (4-[3-chloroanilino]-6,7-dimethoxyquinazoline)], and liquid-liquid extraction was performed by addition of 10 volumes of ethyl acetate. After extraction, the supernatant organic layer was transferred to a microcentrifuge tube and dried under a gentle stream of nitrogen. The dried sample was reconstituted in 100 μl of mobile phase, vortex mixed, centrifuged, and transferred to auto sampler

vials, and a 5-μl sample was injected onto a Zorbax Eclipse XDB-C18 column (4.6 × 50 mm, 1.8-μm particle size; Agilent Technologies, Santa Clara, CA). The aqueous mobile phase (A) was 20 mM ammonium formate with 0.1% formic acid, and the organic mobile phase (B) was acetonitrile. The gradient was as follows: 50% B for the first 3 minutes, increased to 90% B from 3 to 3.5 minutes, maintained at 90% B for 3 minutes, and decreased to 50% B within 0.5 minutes. The total run time was 11 minutes with a flow rate of 0.35 ml/min. The ionization was conducted in positive mode, and the m/z transitions were 520.122 → 307.007 and 316.068 → 299.993 for dabrafenib and AG1478, respectively. The retention time of dabrafenib was 6.8 minutes and that of AG1478 was 2.8 minutes. The assay was sensitive and linear over a range of 2 ng/ml to 2 μg/ml, with the coefficient of variation being less than 20% over the entire range.

Pharmacokinetic Calculations. Pharmacokinetic parameters and metrics from the concentration-time data in plasma and brain were obtained by noncompartmental analysis performed using Phoenix WinNonlin 6.2 (Pharsight, Mountain View, CA). The area under the concentration-time profiles for plasma (AUC_{plasma}) and brain (AUC_{brain}) were calculated using the linear trapezoidal method. The sparse sampling module in WinNonlin 6.2 was used to estimate the standard error around the mean of the AUCs (Bailer, 1988; Nedelman et al., 1995).

Statistical Analysis. Data in all experiments represent the mean ± S.D. unless otherwise indicated. One-way analysis of variance, followed by Bonferroni's multiple comparisons test, was used to compare multiple groups. Comparisons between two groups were made using an unpaired t test. A significance level of $P < 0.05$ was used for all experiments. (GraphPad Prism 5.01 software; GraphPad, San Diego, CA).

Results

In Vitro Accumulation of Dabrafenib in MDCKII-Bcrp1 and MDCKII-MDR1 Cells. The cellular accumulation of dabrafenib in MDCKII-wild-type, Bcrp1-transfected, and MDR1-transfected cell lines is summarized in Fig. 2. [^{3}H]-Prazosin and [^{3}H]-vinblastine were used as positive controls for Bcrp and MDR1, respectively, and as expected, the cellular accumulation of these probe substrates was significantly lower as compared with wild-type controls (WT: 100 ± 8; Bcrp1: 16.7 ± 1.4; MDR1: 11.6 ± 3.1), confirming significant transporter activity in these transfected cell lines. We chose a concentration of 2 μM for dabrafenib accumulation studies, as the pilot studies revealed that no saturation of transporters occurs up to 75 μM of dabrafenib (Supplemental Fig. 1). Dabrafenib accumulation was significantly lower in Bcrp1 cells (Fig. 2A; Bcrp: 11.3 ± 1.4; WT: 100 ± 10; $P < 0.001$) when compared with corresponding wild-type controls. The addition of 0.2 μM Ko143, a specific Bcrp1 inhibitor, increased dabrafenib accumulation, such that it was not significantly different from the wild-type controls. Likewise, dabrafenib accumulation in MDR1-transfected cell lines (Fig. 2B) was ~65% lower when compared with wild-type controls, and the difference was abolished when 1 μM LY335979 was used. These data indicate that dabrafenib is a substrate for both P-gp and Bcrp1, and inhibition of these efflux transporters enhances the cellular delivery of dabrafenib.

Competition Assays Using Prototypical Probe Substrates. The effect of increasing concentrations of dabrafenib on the cellular accumulation of prototypical probe substrates (prazosin or mitoxantrone for Bcrp, vinblastine for P-gp) was assessed in MDCKII–wild-type, Bcrp1-transfected, and MDR1-transfected cell lines. Increasing concentrations of

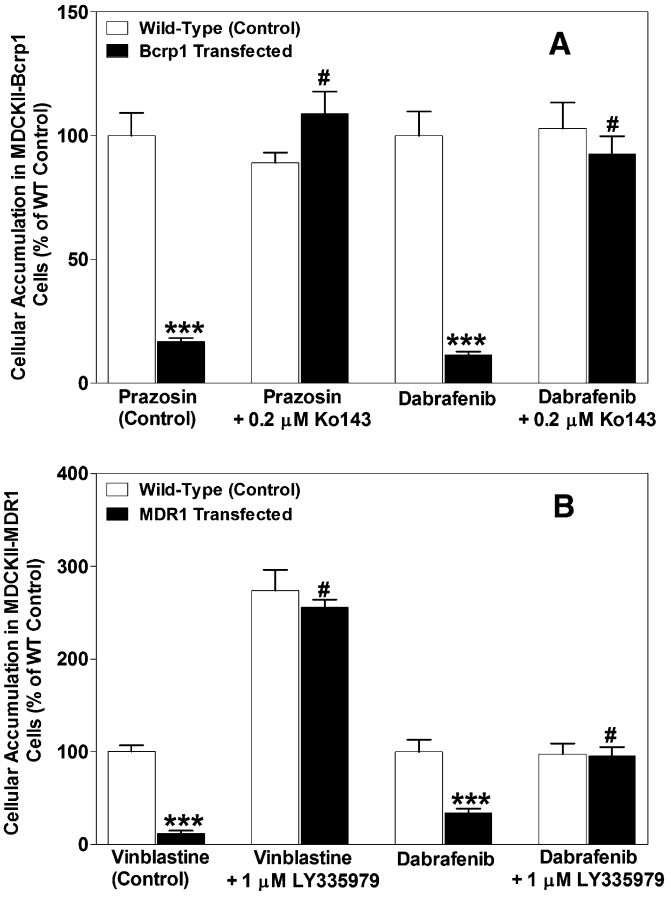

Fig. 2. In vitro cellular accumulation of dabrafenib. (A) The accumulation of prazosin (prototypical Bcrp probe substrate; positive control) and dabrafenib in MDCKII–wild-type and Bcrp1-transfected cell lines with and without Bcrp inhibitor Ko143 (0.2 μM). The accumulation of dabrafenib and vinblastine (probe substrate for P-gp) in MDR1 cells with and without P-gp inhibitor LY335979 (1 μM) is shown in (B). Data represent the mean ± S.D.; $n = 6$ for all data points. ***$P < 0.001$ compared with respective wild-type controls; #$P < 0.001$ compared with the untreated transfected cell line.

dabrafenib did not increase the accumulation of [^{3}H]-prazosin in Bcrp cells or the respective wild-type control cells (Fig. 3A). Similarly, increasing dabrafenib concentrations did not increase the accumulation of [^{3}H]-vinblastine until 25 μM was reached; however, at 50 μM dabrafenib, vinblastine accumulation increased ~1.5- and 2.5-fold in wild-type and MDR1 cells, respectively (Fig. 3B). Furthermore, dabrafenib did not change the cellular accumulation of mitoxantrone in Bcrp1 cells (Supplemental Fig. 2).

Directional Transport Studies. The directional transport of dabrafenib was assessed using monolayers of MDCKII–wild-type, Bcrp1-transfected, and MDR1-transfected lines grown on Transwell permeable membranes. Confluent monolayers were formed in 3–4 days with intact tight junctions. Paracellular leakage was assessed by measuring the transport of [^{14}C]-inulin across the cell monolayers, and the inulin transported in 60 minutes was found to be less than 1%. The directional permeability of dabrafenib was very similar between the A-to-B and B-to-A directions in the wild-type cells (11.5 ± 1.4 versus 14.1 ± 1.4 × 10^{-6} cm/s, respectively; Table 1). However in the Bcrp1-transfected cell line, the apparent permeability of dabrafenib in the B-to-A direction

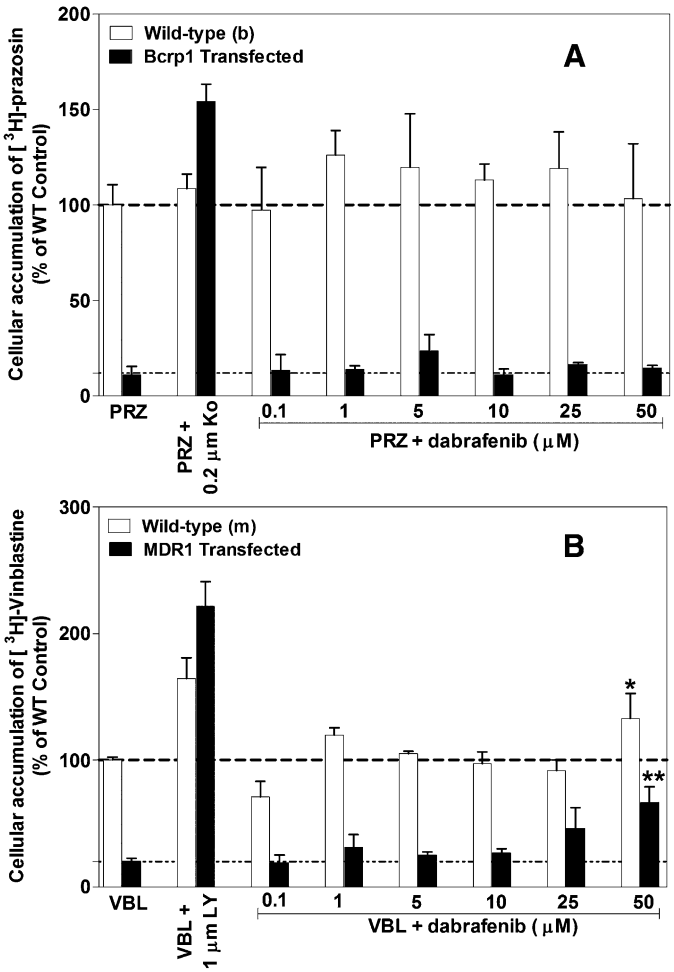

Fig. 3. Competition assays using prototypical probe substrate molecules. Intracellular accumulation of [^{3}H]-prazosin (PRZ; Bcrp probe substrate), [^{3}H]-vinblastine (VBL; P-gp probe substrate) in Bcrp1-transfected (A) and MDR1-transfected (B) cell lines with increasing concentrations of dabrafenib from 0.1 to 50 μM. Ko: Bcrp inhibitor Ko143; LY: P-gp inhibitor LY335979. Data represent the mean ± S.D.; $n = 3$ for all data points. *$P = 0.0439$ compared with untreated wild-type cells; **$P = 0.003$ compared with untreated MDR1 cells.

was significantly higher than the permeability in the A-to-B direction (A-to-B: 1.3 ± 0.3; B-to-A: 27.3 ± 4.1; $P < 0.05$; Table 1) with an efflux ratio of 21. Treatment with Ko143 significantly ($P < 0.05$) reduced the Bcrp1-mediated efflux of dabrafenib in the B-to-A direction and increased the A-to-B permeability with a resulting efflux ratio of 0.7. The corrected efflux ratio was found to be ~18 for Bcrp1-mediated transport. Similarly, in MDR1 cells, the B-to-A permeability was significantly higher compared with A-to-B permeability, with an efflux ratio of 11. Addition of LY335979, a specific P-gp inhibitor, abolished the difference in directional permeabilities with a resulting efflux ratio of 1 (Table 2). The corrected efflux ratio was ~4. These results conclusively indicate that dabrafenib is an avid substrate for both Bcrp1 and P-gp.

Plasma Protein and Brain Tissue Binding. Since it is the unbound drug concentration that results in pharmacological action, we determined the free fraction (f_u) in plasma and brain tissue homogenates. Dabrafenib is highly bound to plasma proteins as well as brain tissue. No significant difference was observed in free fraction in plasma and brain tissue homogenate when compared between wild-type and *Mdr1a/b*$^{-/-}$*Bcrp1*$^{-/-}$ mice genotypes (wild-type: $f_{u,\ plasma} = 0.004 \pm 0.001$, $f_{u,brain\ homogenate} = 0.02 \pm 0.003$; *Mdr1a/b*$^{-/-}$*Bcrp1*$^{-/-}$: $f_{u,\ plasma} = 0.006 \pm 0.004$, ($f_{u,brain\ homogenate} = 0.02 \pm 0.005$).

Brain Distribution of Dabrafenib in FVB Wild-Type and Mdr1a/b$^{-/-}$Bcrp1$^{-/-}$ Mice. The brain and plasma dabrafenib concentration time profiles after an i.v. dose of 2.5 mg/kg in FVB wild-type mice are summarized in Fig. 4. The brain concentrations of dabrafenib were significantly lower than the corresponding plasma concentrations at all measured time points. The pharmacokinetic parameters are summarized in Table 3. The brain-to-plasma partitioning (K_p; AUC_{brain} / AUC_{plasma}) was found to be 0.023, indicating the limited distribution of dabrafenib to the brain. We also investigated the brain distribution of dabrafenib in *Mdr1a/b*$^{-/-}$*Bcrp1*$^{-/-}$ mice after a 2.5-mg/kg i.v. dose of dabrafenib. The plasma concentrations were no different between wild-type and *Mdr1a/b*$^{-/-}$*Bcrp1*$^{-/-}$ mice (Fig. 5A); however, the brain concentrations of dabrafenib in *Mdr1a/b*$^{-/-}$*Bcrp1*$^{-/-}$ mice (Fig. 5B) were significantly higher than the corresponding brain concentrations observed in wild-type mice. The K_p in *Mdr1a/b*$^{-/-}$*Bcrp1*$^{-/-}$ mice increased to ~0.4, which was 18-fold greater than what was observed in wild-type mice, indicating the influence of P-gp, Bcrp, or both on the brain distribution of dabrafenib.

Dabrafenib is administered to patients orally (Falchook et al., 2012), and we sought to determine the brain and plasma pharmacokinetics after an oral dose. Hence, in a separate study, we investigated the brain distribution of dabrafenib after an oral dose of 25 mg/kg in wild-type and *Mdr1a/b*$^{-/-}$*Bcrp1*$^{-/-}$ mice, and the results are summarized in Fig. 6 and Table 4. The AUC_{plasma} in *Mdr1a/b*$^{-/-}$*Bcrp1*$^{-/-}$ mice (31 ± 5 μg × min/ml) was

TABLE 1
Directional flux of dabrafenib in MDCKII-WT– and MDCKII-Bcrp1–transfected cell lines
Data represent the mean ± S.D. ($n = 3$).

Cell Line	P_{app}		ER	CFR
	A-to-B	B-to-A		
	cm/s ×10^{-6}	*cm/s* ×10^{-6}		
MDCKII-WT	11.5 ± 1.4	14.1 ± 1.4	1.2	—
MDCKII-WT + 0.2 μM Ko143	16.4 ± 0.9	15.3 ± 2.6	0.9	
MDCKII-Bcrp1	1.3 ± 0.3[a]	27.3 ± 4.1[a]	21.0	17.5
MDCKII-Bcrp1 + 0.2 μM Ko143	13.2 ± 2.1[b]	9.6 ± 0.33[b]	0.7	

A, apical; B, basolateral; Bcrp1, breast cancer resistance protein 1; CFR, corrected efflux ratio; ER, efflux ratio; MDCKII, Madin-Darby canine kidney II; P_{app}, apparent permeability of dabrafenib; WT, wild type.
[a] Significantly different compared with respective wild-type control cells.
[b] Significantly different compared with untreated Bcrp1 control cells.

TABLE 2
Directional flux of dabrafenib in MDCKII-WT and MDCKII-MDR1 cells
Data represent the mean ± S.D. (n = 3).

Cell Line	P_{app}		ER	CFR
	A-to-B	B-to-A		
	$cm/s \times 10^{-6}$	$cm/s \times 10^{-6}$		
MDCKII-WT	2.6 ± 1.0	7.7 ± 1.6	3.0	—
MDCKII-WT + 1 μM LY335979	5.5 ± 0.4	5.2 ± 0.7	0.90	
MDCKII-MDR1	0.7 ± 0.3[a]	7.9 ± 1.9	11.4	3.8
MDCKII-MDR1 + 1 μM LY335979	4.9 ± 0.52[b]	5.2 ± 1.4	1.1	

A, apical; B, basolateral; CFR, corrected efflux ratio; ER, efflux ratio; MDCKII, Madin-Darby canine kidney II; P_{app}, apparent permeability of dabrafenib; WT, wild type.
[a] Significantly different compared with respective wild-type control cells.
[b] Significantly different compared with untreated MDR1 control cells.

~2-fold higher compared with the wild-type mice (16 ± 3 μg × min/ml). This indicates that P-gp and Bcrp may have some influence on the oral absorption or systemic clearance of dabrafenib at a 25 mg/kg dose. Dabrafenib brain concentrations were significantly enhanced in *Mdr1a/b*$^{-/-}$*Bcrp1*$^{-/-}$ mice compared with those in wild-type mice. The AUC_{brain} in wild-type mice was 0.69 μg × min/ml, which increased approximately 10-fold in *Mdr1a/b*$^{-/-}$*Bcrp1*$^{-/-}$ to 7.6 μg × min/ml. The K_p in wild-type mice was 0.044, which increased 6-fold in *Mdr1a/b*$^{-/-}$*Bcrp1*$^{-/-}$ mice to 0.25. The aggregate of these data suggests that the brain distribution of dabrafenib is significantly limited at the BBB due to active efflux by both P-gp and BCRP after either intravenous or oral administration.

Comparison of Brain Distribution of Dabrafenib with Vemurafenib. We compared the brain distribution of dabrafenib after a single oral dose with our previously published results for vemurafenib (Mittapalli et al., 2012), and the data are shown in Fig. 7. The plasma concentrations, for both dabrafenib and vemurafenib, were higher in the *Mdr1a/b*$^{-/-}$*Bcrp1*$^{-/-}$ mice compared with wild-type mice (Fig. 7A). It should be noted that the plasma concentrations of dabrafenib were not significantly different as compared with vemurafenib in either type of mice. Since the total brain distribution of vemurafenib was approximately equal to the brain vascular volume, for comparison purposes, the data shown in this particular case were not corrected for vascular content for either dabrafenib or vemurafenib. The brain concentrations of dabrafenib were significantly higher compared with vemurafenib brain concentrations in both wild-type and *Mdr1a/b*$^{-/-}$*Bcrp1*$^{-/-}$ mice (Fig. 7B). The brain-to-plasma concentration ratio for dabrafenib is ~10, ~4-fold greater compared with the vemurafenib brain-to-plasma ratio in wild-type and *Mdr1a/b*$^{-/-}$*Bcrp1*$^{-/-}$ mice, respectively [wild-type: 0.1 ± 0.03 (dabrafenib) and 0.008 ± 0.001 (vemurafenib); *Mdr1a/b*$^{-/-}$*Bcrp1*$^{-/-}$: 0.3 ± 0.04 (dabrafenib) and 0.07 ± 0.02 (vemurafenib)]. The aggregate of these data indicates that dabrafenib has greater brain penetration than vemurafenib.

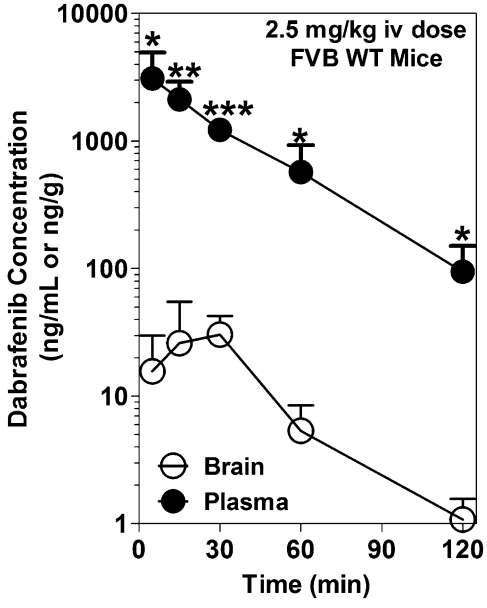

Fig. 4. Brain and plasma concentration versus time profiles of dabrafenib. Brain and plasma concentrations of dabrafenib after an i.v. dose of 2.5 mg/kg in FVB wild-type mice at 5, 15, 30, 60, and 120 minutes postdose. Brain concentrations of dabrafenib are significantly lower than plasma concentrations at all measured time points. Data represent the mean ± S.D.; n = 3–4. *$P < 0.05$; **$P < 0.001$; ***$P < 0.0001$.

Discussion

Brain metastases are a common cause of death from stage IV metastatic melanoma (Skibber et al., 1996; Davies et al., 2011). Until 2011, the only FDA-approved therapies for metastatic melanoma were dacarbazine and interleukin-2, which showed response rates of only 10–20% (Comis, 1976; Atkins et al., 1999; Garbe et al., 2011). However, therapies for metastatic melanoma have been changed dramatically with the development of highly selective inhibitors of $BRAF^{V600E}$, the most commonly found mutation in melanoma patients. The first of these selective $BRAF^{V600E}$ inhibitors, vemurafenib, was approved by the U.S. FDA in 2011, and showed remarkable efficacy in clinical trials (Chapman et al., 2011). A second $BRAF^{V600E}$ inhibitor, dabrafenib, showed similar results when compared with vemurafenib, with fewer adverse effects in clinical trials (Falchook et al., 2012; Hauschild et al., 2012). Further, dabrafenib showed remarkable efficacy in reducing tumor size in the brains of patients with brain metastases (Falchook et al., 2012). However, a durable response depends on effective delivery of therapies to all sites of metastases in the brain, especially to the micrometastases (less than 1 mm in diameter) that have an intact BBB (Gibney and Sondak, 2012) with functional efflux transporters. Furthermore, in a recent study, Rochet et al. (2012) reported that treatment of melanoma patients with vemurafenib

TABLE 3
Comparison of pharmacokinetic parameters of dabrafenib in FVB wild-type and *Mdr1a/b*$^{-/-}$*Bcrp1*$^{-/-}$ mice after an i.v. dose of 2.5 mg/kg

	Wild Type		*Mdr1a/b*$^{-/-}$*Bcrp1*$^{-/-}$ Mice	
	Plasma	Brain	Plasma	Brain
Terminal rate constant (min^{-1})	0.03	0.036	0.024	0.026
Half-life (min)	23.7	19.1	28.3	26.6
Clearance (ml/min/kg)	24.2		28.4	
Volume of distribution (l/kg)	0.83		1.2	
$AUC_{0 \rightarrow t\ last}$ (μg · min /ml)[a]	120.9 ± 15.8	2.8 ± 0.4	101.4 ± 8.7	42.1 ± 3.4[b]
K_p	0.023		0.42	
K_p ratio[c]	18.3			

AUC, area under the concentration-time curve; FVB, Friend leukemia virus strain B; K_p, AUC_{brain}/AUC_{plasma}.
[a] Area under the curve from time zero to 2 hours postdose.
[b] $P < 0.05$ compared with wild-type AUC_{brain}.
[c] K_p ratio = (K_p in *Mdr1a/b*$^{-/-}$*Bcrp1*$^{-/-}$ mice) / (K_p in wild-type mice).

resulted in development of metastatic disease in the brain. From these data, it appears that the brain remains at least in part a pharmacological sanctuary site due to the continued presence of an intact BBB where some metastatic sites reside. The efficacy of dabrafenib in brain metastases of melanoma is under investigation in a phase 2 clinical trial. With this perspective, it is critical to determine the mechanisms that limit the brain distribution of dabrafenib. In the current study, using both in vitro and in vivo models, we demonstrate that dabrafenib is a dual substrate for BCRP and P-gp, and its brain distribution is limited due to active efflux at the BBB. Furthermore, our data indicate that dabrafenib has greater brain distribution when compared with vemurafenib, and as such, dabrafenib might have some advantages for treating patients with melanoma brain metastases. To the best of our knowledge, this is the first report to show the brain distribution of dabrafenib and its interactions with Bcrp and P-gp.

The experiments performed in transfected MDCKII cells that overexpress either murine Bcrp or human P-gp revealed that dabrafenib is a dual substrate for both Bcrp and P-gp (Fig. 2; Tables 1 and 2). Interestingly, inhibition studies conducted using prototypical probe substrates (prazosin and mitoxantrone for Bcrp, and vinblastine for P-gp) showed no increase in probe substrate accumulation with increasing concentrations of dabrafenib up to a concentration of 50 and 25 μM in Bcrp1 and MDR1 cells, respectively. In both wild-type and MDR1 cells, using vinblastine as a probe substrate, dabrafenib showed a significant increase in accumulation at 50 μM. However, it should be noted that this concentration is not pharmacologically relevant, as the clinically observed concentrations of dabrafenib (150 mg/kg twice daily) are ~2 μM (Falchook et al., 2012).

Specific Bcrp (Ko143) and P-gp (LY335979) inhibitors were able to increase cellular accumulation of dabrafenib (Fig. 2), as well as the probe substrates (Fig. 3), in both Bcrp1 and MDR1 cells, respectively, indicating that Ko143 and LY335979 bind to multiple binding sites on the transporter proteins. The fact that dabrafenib is a substrate for both Bcrp and P-gp, but does not inhibit these transporter proteins for some prototypical probe substrates, may indicate that dabrafenib binds to a different site on the transporter protein as compared with the probe substrates tested. It is noteworthy to recognize how screening assays using specific binding-site probe substrates can be misleading. In our previous studies, we have shown that differences exist in the inhibition of BCRP depending on both the inhibitor used and the substrate under evaluation (Giri et al., 2009).

With this knowledge from in vitro data, we next investigated the in vivo brain distribution of dabrafenib in

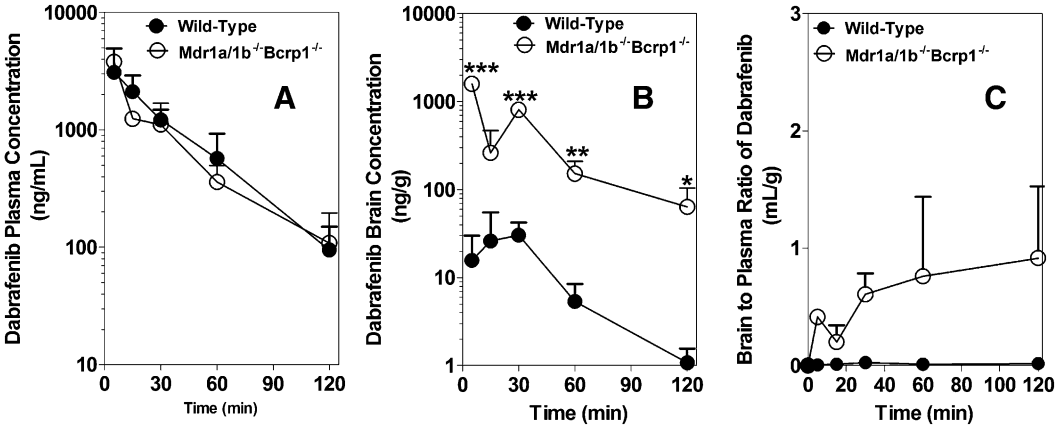

Fig. 5. Brain distribution of dabrafenib in FVB wild-type and *Mdr1a/b*$^{-/-}$*Bcrp1*$^{-/-}$ mice. Plasma concentration versus time (A), brain concentration versus time (B), and brain-to-plasma concentration ratios (C) of dabrafenib in wild-type and *Mdr1a/b*$^{-/-}$*Bcrp1*$^{-/-}$ mice after an i.v. dose of 2.5 mg/kg. Plasma and brain concentrations were determined using LC-MS/MS at 5, 15, 30, 60, and 120 minutes postdose of dabrafenib. Data represent the mean ± S.D.; n = 3–4. *$P < 0.05$; **$P < 0.001$; ***$P < 0.0001$.

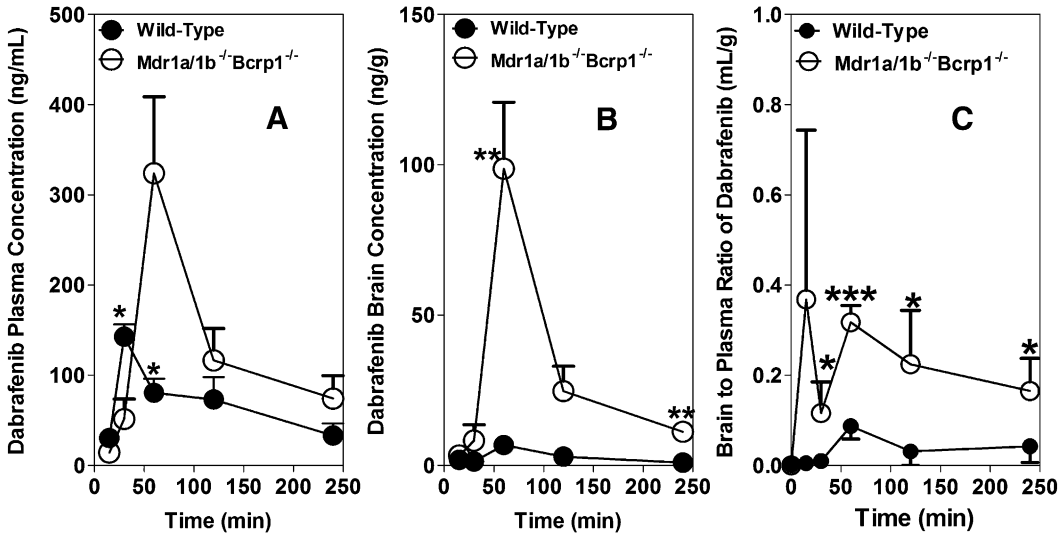

Fig. 6. Brain distribution of dabrafenib in FVB wild-type and *Mdr1a/b*$^{-/-}$*Bcrp1*$^{-/-}$ mice after an oral dose. Plasma (A) and brain (B) concentration versus time profiles, and brain-to-plasma concentration ratios (C) of dabrafenib in wild-type and *Mdr1a/b*$^{-/-}$*Bcrp1*$^{-/-}$ mice after an oral dose of 25 mg/kg. Plasma and brain concentrations were determined using LC-MS/MS at 15, 30, 60, 120, and 240 minutes postdose of dabrafenib. Data represent the mean ± S.D.; n = 3–4. *$P < 0.05$; **$P < 0.001$; ***$P < 0.0001$.

mice. After an i.v. dose, the brain concentrations of dabrafenib in FVB wild-type mice were significantly lower than the corresponding plasma concentrations (Fig. 4), with a K_p of 0.023. However, the brain distribution of dabrafenib was significantly improved when the same dose was administered in *Mdr1a/b*$^{-/-}$*Bcrp1*$^{-/-}$ mice, with a resulting K_p of 0.42 (Table 3). It is worth noting that the unbound brain-to-plasma partition ratios [($K_{p,uu}$) ratio of unbound drug in brain to unbound drug in plasma] in wild-type and *Mdr1a/b*$^{-/-}$*Bcrp1*$^{-/-}$ mice were ~0.1 and ~1.7, respectively. These data indicate that dabrafenib brain distribution is limited in an intact BBB model through the action of efflux transporter–mediated clearance.

Since the clinical use of dabrafenib involves chronic multiple oral dosing, we next determined the brain distribution of dabrafenib after oral administration. The AUC_{plasma} in *Mdr1a/b*$^{-/-}$*Bcrp1*$^{-/-}$ mice is ~2-fold higher (Fig. 6A; Table 4) compared with wild-type mice after oral administration. As the systemic clearance is no different between the genotypes after an i.v. dose (see Fig. 5; Table 3), the observed higher plasma exposure in Mdr1a/b−/−Bcrp1−/− mice after the oral dose indicates that BCRP and P-gp may have some influence on oral absorption of dabrafenib at a 25-mg/kg dose. This phenomenon was observed with other drugs that are dual substrates of BCRP and P-gp, such as dasatinib (Lagas et al., 2009) and vemurafenib (Durmus et al., 2012). However, the AUC_{brain} in *Mdr1a/b*$^{-/-}$*Bcrp1*$^{-/-}$ mice is ~12 fold higher when compared to wild-type mice resulting in a K_p ratio of ~6. Taken together, all of these data indicate that dabrafenib brain distribution is limited in an intact BBB model. In this regard, use of pharmacological inhibitors such as elacridar, a dual P-gp and Bcrp inhibitor, may have significant value in improving the CNS distribution of dabrafenib.

Since both dabrafenib and vemurafenib are showing remarkable results in clinical trials, it is appropriate to compare these two molecules in terms of their brain distribution. In our previous study, we have shown that both BCRP and P-gp have a significant impact on the brain distribution of vemurafenib (Mittapalli et al., 2012), which was further supported by a recently published report by another group (Durmus et al., 2012). Compared with vemurafenib (Mittapalli et al., 2012), the B/P ratio of dabrafenib is significantly higher in both wild-type and *Mdr1a/b*$^{-/-}$*Bcrp1*$^{-/-}$ mice (Fig. 7). Although the B/P ratio in this case was measured only at one time point, we also

TABLE 4

Pharmacokinetic metrics in FVB wild-type and *Mdr1a/b*$^{-/-}$*Bcrp1*$^{-/-}$ mice after oral dosing with 25 mg/kg dabrafenib

Data are presented as the mean ± S.D.

Mouse Genotype	Tissue	C_{max}	AUC_{last}[a]	K_p	K_p Ratio[b]
		$\mu g/ml$	$\mu g \times min/ml$		
Wild-type	Plasma	0.143 ± 0.014	15.8 ± 3.0	0.044	5.7
Wild-type	Brain	0.007 ± 0.001	0.69 ± 0.22		
Mdr1a/b$^{-/-}$*Bcrp1*$^{-/-}$	Plasma	0.324 ± 0.085	31.1 ± 5.1[c]	0.25	
Mdr1a/b$^{-/-}$*Bcrp1*$^{-/-}$	Brain	0.098 ± 0.022	7.6 ± 1.3[d]		

AUC, area under the curve; FVB, Friend leukemia virus strain B; K_p, AUC_{brain}/AUC_{plasma}.
[a] Area under the curve from time zero to 4 hours postdose.
[b] K_p in *Mdr1a/b*$^{-/-}$*Bcrp1*$^{-/-}$ mice/K_p in wild-type mice.
[c] $P = 0.0414$ compared with wild-type plasma.
[d] $P = 0.002$ compared with wild-type brain.

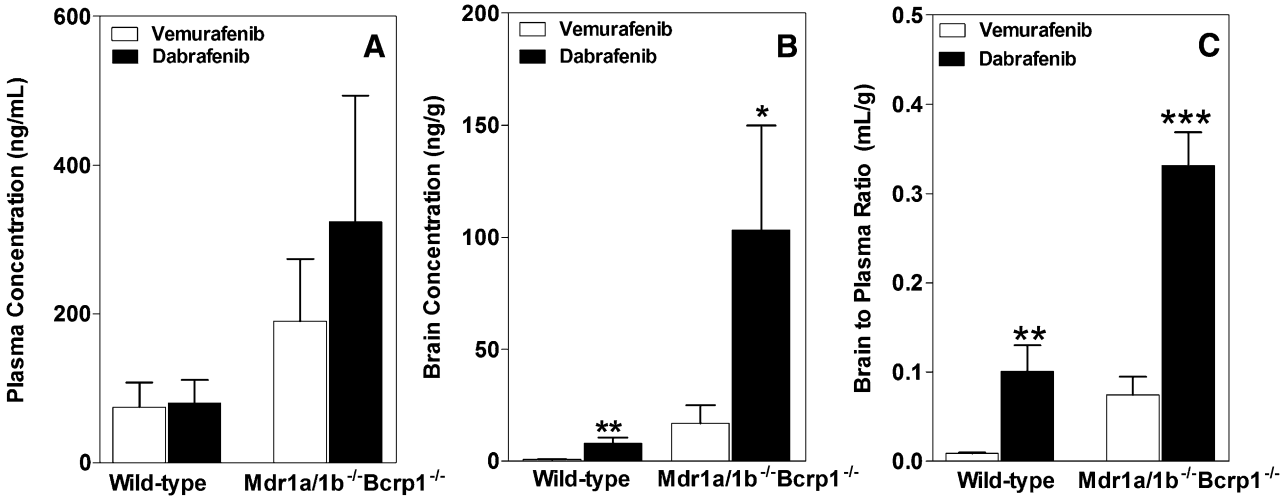

Fig. 7. Comparison of the brain distribution of dabrafenib and vemurafenib. Plasma (A), brain (B), and brain-to-plasma concentration ratios (C) of dabrafenib and vemurafenib in wild-type and *Mdr1a/b*$^{-/-}$*Bcrp1*$^{-/-}$ mice after 1 hour postdose in separate animals (25 mg/kg, oral dose). Vemurafenib data are from our previously published results (Mittapalli et al., 2012). Data represent the mean ± S.D.; n = 3–4. *$P < 0.05$; **$P < 0.001$; ***$P < 0.0001$.

observed a greater AUC_{brain} to AUC_{plasma} ratio of dabrafenib in wild-type mice after a similar i.v. dose as compared with vemurafenib (Table 5). Given the in vitro potency of dabrafenib, which is at least 40 times higher than vemurafenib against $BRAF^{V600E}$ [vemurafenib IC_{50}: 31 nM (Bollag et al., 2010); dabrafenib IC_{50}: 0.8 nM (Laquerre et al., 2009)], and greater brain penetration than vemurafenib, dabrafenib might be beneficial in treating melanoma brain metastases; however, this prediction warrants further preclinical and clinical investigation.

Currently, the duration of response with single-agent therapy has been limited because the development of resistance is inevitable, as reported in the case of vemurafenib (Johannessen et al., 2010; Nazarian et al., 2010; Villanueva et al., 2010). Further, studies have shown that mutations in upstream signaling proteins such as RAS or compensatory signaling from other growth factor receptors such as PI3K/mTOR drive the reactivation of the MAPK signaling pathway and build up the resistance to BRAF therapy (Flaherty et al., 2012). Thus, understanding the key molecular aberrations associated with resistance will be crucial in designing the rational combinations using two or more drugs to simultaneously block multiple pathways, such as the clinical trial evaluating the combination of dabrafenib with the MEK inhibitor trametinib (NCT01072175). Also, the evaluation of combinations of immune therapies such as ipilimumab (Margolin et al., 2012) and rational choices of molecularly targeted agents would be valuable in overcoming the low response rates of immune therapy and short durations of response associated with targeted therapies.

The development of $BRAF^{V600E}$ inhibitors has been a major breakthrough for the treatment of melanoma patients. However, challenges still remain in delivering these targeted therapies to melanoma micrometastases in the brain that could be growing behind an intact BBB. Given the success rate so far with both dabrafenib and vemurafenib, it will be essential to determine both the resistance mechanisms and CNS delivery issues that need to be addressed to achieve a durable response. Multiple drugs/cocktails need to be evaluated for rational combinations (e.g., a BRAF inhibitor and/or MEK inhibitor and/or PI3K/mTOR inhibitor) to decrease resistance in peripheral or systemic disease. At the same time, there is also a critical need to examine the CNS delivery of combinations to see if one agent influences the brain delivery of another, or if one or more drug(s) in the combination does not reach the brain, leading to heightened resistance. The successful and durable treatment of melanoma requires that the brain does not become a pharmacological sanctuary site for melanoma metastases.

TABLE 5
Comparison of brain distribution of vemurafenib and dabrafenib in FVB wild-type mice after an i.v. dose of 2.5 mg/kg

	Dabrafenib		Vemurafenib[a]	
	Plasma	Brain	Plasma	Brain
Terminal rate constant (min^{-1})	0.031	0.036	0.0051	0.0047
Half-life (min)	23.7	19.1	136	148
Clearance (ml/min/kg)	24.2		1.6	
Volume of distribution (l/kg)	0.83		0.316	
$AUC_{0 \rightarrow t\ last}$ (min · μg/ml)	120.9 ± 15.8	2.8 ± 0.4	1663 ± 140	6.5 ± 0.9
K_p	0.023		0.004	

AUC, area under the concentration-time curve; FVB, Friend leukemia virus strain B; K_p, AUC_{brain}/AUC_{plasma}.
[a] From previously published data (Mittapalli et al., 2012).

Acknowledgments

The authors thank Jim Fisher, Clinical Pharmacology Analytical Services Laboratory, University of Minnesota, for help and support in the development of the dabrafenib LC-MS/MS assay.

Authorship Contributions

Participated in research design: Mittapalli, Vaidhyanathan, Dudek, Elmquist.

Conducted experiments: Mittapalli, Vaidhyanathan.

Performed data analysis: Mittapalli, Elmquist.

Wrote or contributed to the writing of the manuscript: Mittapalli, Dudek, Elmquist.

References

Agarwal S, Sane R, Gallardo JL, Ohlfest JR, and Elmquist WF (2010) Distribution of gefitinib to the brain is limited by P-glycoprotein (ABCB1) and breast cancer resistance protein (ABCG2)-mediated active efflux. *J Pharmacol Exp Ther* **334**: 147–155.

Agarwal S, Sane R, Ohlfest JR, and Elmquist WF (2011) The role of the breast cancer resistance protein (ABCG2) in the distribution of sorafenib to the brain. *J Pharmacol Exp Ther* **336**:223–233.

Atkins MB, Lotze MT, Dutcher JP, Fisher RI, Weiss G, Margolin K, Abrams J, Sznol M, Parkinson D, and Hawkins M, et al. (1999) High-dose recombinant interleukin 2 therapy for patients with metastatic melanoma: analysis of 270 patients treated between 1985 and 1993. *J Clin Oncol* **17**:2105–2116.

Bailer AJ (1988) Testing for the equality of area under the curves when using destructive measurement techniques. *J Pharmacokinet Biopharm* **16**:303–309.

Bollag G, Hirth P, Tsai J, Zhang J, Ibrahim PN, Cho H, Spevak W, Zhang C, Zhang Y, and Habets G, et al. (2010) Clinical efficacy of a RAF inhibitor needs broad target blockade in BRAF-mutant melanoma. *Nature* **467**:596–599.

Chapman PB, Hauschild A, Robert C, Haanen JB, Ascierto P, Larkin J, Dummer R, Garbe C, Testori A, and Maio M, et al.; BRIM-3 Study Group (2011) Improved survival with vemurafenib in melanoma with BRAF V600E mutation. *N Engl J Med* **364**:2507–2516.

Comis RL (1976) DTIC (NSC-45388) in malignant melanoma: a perspective. *Cancer Treat Rep* **60**:165–176.

Dai H, Marbach P, Lemaire M, Hayes M, and Elmquist WF (2003) Distribution of STI-571 to the brain is limited by P-glycoprotein-mediated efflux. *J Pharmacol Exp Ther* **304**:1085–1092.

Davies H, Bignell GR, Cox C, Stephens P, Edkins S, Clegg S, Teague J, Woffendin H, Garnett MJ, and Bottomley W, et al. (2002) Mutations of the BRAF gene in human cancer. *Nature* **417**:949–954.

Davies MA, Liu P, McIntyre S, Kim KB, Papadopoulos N, Hwu WJ, Hwu P, and Bedikian A (2011) Prognostic factors for survival in melanoma patients with brain metastases. *Cancer* **117**:1687–1696.

de Vries NA, Zhao J, Kroon E, Buckle T, Beijnen JH, and van Tellingen O (2007) P-glycoprotein and breast cancer resistance protein: two dominant transporters working together in limiting the brain penetration of topotecan. *Clin Cancer Res* **13**:6440–6449.

Deeken JF and Löscher W (2007) The blood-brain barrier and cancer: transporters, treatment, and Trojan horses. *Clin Cancer Res* **13**:1663–1674.

Durmus S, Sparidans RW, Wagenaar E, Beijnen JH, and Schinkel AH (2012) Oral availability and brain penetration of the B-RAF(V600E) inhibitor vemurafenib can be enhanced by the P-glycoprotein (ABCB1) and breast cancer resistance protein (ABCG2) inhibitor elacridar. *Mol Pharm* **9**:3236–3245.

Falchook GS, Long GV, Kurzrock R, Kim KB, Arkenau TH, Brown MP, Hamid O, Infante JR, Millward M, and Pavlick AC, et al. (2012) Dabrafenib in patients with melanoma, untreated brain metastases, and other solid tumours: a phase 1 dose-escalation trial. *Lancet* **379**:1893–1901.

Fife KM, Colman MH, Stevens GN, Firth IC, Moon D, Shannon KF, Harman R, Petersen-Schaefer K, Zacest AC, and Besser M, et al. (2004) Determinants of outcome in melanoma patients with cerebral metastases. *J Clin Oncol* **22**:1293–1300.

Flaherty KT, Infante JR, Daud A, Gonzalez R, Kefford RF, Sosman J, Hamid O, Schuchter L, Cebon J, and Ibrahim N, et al. (2012) Combined BRAF and MEK inhibition in melanoma with BRAF V600 mutations. *N Engl J Med* **367**:1694–1703.

Garbe C, Eigentler TK, Keilholz U, Hauschild A, and Kirkwood JM (2011) Systematic review of medical treatment in melanoma: current status and future prospects. *Oncologist* **16**:5–24.

Gibney GT and Sondak VK (2012) Extending the reach of BRAF-targeted cancer therapy. *Lancet* **379**:1858–1859.

Giri N, Agarwal S, Shaik N, Pan G, Chen Y, and Elmquist WF (2009) Substrate-dependent breast cancer resistance protein (Bcrp1/Abcg2)-mediated interactions: consideration of multiple binding sites in in vitro assay design. *Drug Metab Dispos* **37**:560–570.

Hauschild A, Grob JJ, Demidov LV, Jouary T, Gutzmer R, Millward M, Rutkowski P, Blank CU, Miller WH, Jr, and Kaempgen E, et al. (2012) Dabrafenib in BRAF-mutated metastatic melanoma: a multicentre, open-label, phase 3 randomised controlled trial. *Lancet* **380**:358–365.

Hawkins BT and Davis TP (2005) The blood-brain barrier/neurovascular unit in health and disease. *Pharmacol Rev* **57**:173–185.

Johannessen CM, Boehm JS, Kim SY, Thomas SR, Wardwell L, Johnson LA, Emery CM, Stransky N, Cogdill AP, and Barretina J, et al. (2010) COT drives resistance to RAF inhibition through MAP kinase pathway reactivation. *Nature* **468**:968–972.

Kalvass JC, Maurer TS, and Pollack GM (2007) Use of plasma and brain unbound fractions to assess the extent of brain distribution of 34 drugs: comparison of unbound concentration ratios to in vivo p-glycoprotein efflux ratios. *Drug Metab Dispos* **35**:660–666.

Lagas JS, van Waterschoot RA, van Tilburg VA, Hillebrand MJ, Lankheet N, Rosing H, Beijnen JH, and Schinkel AH (2009) Brain accumulation of dasatinib is restricted by P-glycoprotein (ABCB1) and breast cancer resistance protein (ABCG2) and can be enhanced by elacridar treatment. *Clin Cancer Res* **15**:2344–2351.

Laquerre S, Arnone M, Moss K, Yang J, Fisher K, Kane-Carson LS, Smitheman K, Ward J, Heidrich B, and Rheault T, et al. (2009) A selective Raf kinase inhibitor induces cell death and tumor regression of human cancer cell lines encoding B-RafV600E mutation. *Mol Cancer Ther* **8**(12, Suppl)B88.

Lockman PR, Mittapalli RK, Taskar KS, Rudraraju V, Gril B, Bohn KA, Adkins CE, Roberts A, Thorsheim HR, and Gaasch JA, et al. (2010) Heterogeneous blood-tumor barrier permeability determines drug efficacy in experimental brain metastases of breast cancer. *Clin Cancer Res* **16**:5664–5678.

Long GV, Trefzer U, Davies MA, Kefford RF, Ascierto PA, Chapman PB, Puzanov I, Hauschild A, Robert C, and Algazi A, et al. (2012) Dabrafenib in patients with Val600Glu or Val600Lys BRAF-mutant melanoma metastatic to the brain (BREAK-MB): a multicentre, open-label, phase 2 trial. *Lancet Oncol* **13**:1087–1095.

Margolin K, Ernstoff MS, Hamid O, Lawrence D, McDermott D, Puzanov I, Wolchok JD, Clark JI, Sznol M, and Logan TF, et al. (2012) Ipilimumab in patients with melanoma and brain metastases: an open-label, phase 2 trial. *Lancet Oncol* **13**: 459–465.

McCubrey JA, Milella M, Tafuri A, Martelli AM, Lunghi P, Bonati A, Cervello M, Lee JT, and Steelman LS (2008) Targeting the Raf/MEK/ERK pathway with small-molecule inhibitors. *Curr Opin Investig Drugs* **9**:614–630.

Mittapalli RK, Vaidhyanathan S, Sane R, and Elmquist WF (2012) Impact of P-glycoprotein (ABCB1) and breast cancer resistance protein (ABCG2) on the brain distribution of a novel BRAF inhibitor: vemurafenib (PLX4032). *J Pharmacol Exp Ther* **342**:33–40.

Nazarian R, Shi H, Wang Q, Kong X, Koya RC, Lee H, Chen Z, Lee MK, Attar N, and Sazegar H, et al. (2010) Melanomas acquire resistance to B-RAF(V600E) inhibition by RTK or N-RAS upregulation. *Nature* **468**:973–977.

Nedelman JR, Gibiansky E, and Lau DT (1995) Applying Bailer's method for AUC confidence intervals to sparse sampling. *Pharm Res* **12**:124–128.

Polli JW, Olson KL, Chism JP, John-Williams LS, Yeager RL, Woodard SM, Otto V, Castellino S, and Demby VE (2009) An unexpected synergist role of P-glycoprotein and breast cancer resistance protein on the central nervous system penetration of the tyrosine kinase inhibitor lapatinib (N-3-chloro-4-[(3-fluorobenzyl)oxy]phenyl-6-[5-([2-(methylsulfonyl)ethyl]aminomethyl)-2-furyl]-4-quinazolinamine; GW572016). *Drug Metab Dispos* **37**:439–442.

Rochet NM, Dronca RS, Kottschade LA, Chavan RN, Gorman B, Gilbertson JR, and Markovic SN (2012) Melanoma brain metastases and vemurafenib: need for further investigation. *Mayo Clin Proc* **87**:976–981.

Schinkel AH and Jonker JW (2003) Mammalian drug efflux transporters of the ATP binding cassette (ABC) family: an overview. *Adv Drug Deliv Rev* **55**:3–29.

Siegel R, Ward E, Brawley O, and Jemal A (2011) Cancer statistics, 2011: the impact of eliminating socioeconomic and racial disparities on premature cancer deaths. *CA Cancer J Clin* **61**:212–236.

Skibber JM, Soong SJ, Austin L, Balch CM, and Sawaya RE (1996) Cranial irradiation after surgical excision of brain metastases in melanoma patients. *Ann Surg Oncol* **3**:118–123.

Sosman JA, Kim KB, Schuchter L, Gonzalez R, Pavlick AC, Weber JS, McArthur GA, Hutson TE, Moschos SJ, and Flaherty KT, et al. (2012) Survival in BRAF V600-mutant advanced melanoma treated with vemurafenib. *N Engl J Med* **366**: 707–714.

Tsao H, Atkins MB, and Sober AJ (2004) Management of cutaneous melanoma. *N Engl J Med* **351**:998–1012.

Villanueva J, Vultur A, Lee JT, Somasundaram R, Fukunaga-Kalabis M, Cipolla AK, Wubbenhorst B, Xu X, Gimotty PA, and Kee D, et al. (2010) Acquired resistance to BRAF inhibitors mediated by a RAF kinase switch in melanoma can be overcome by cotargeting MEK and IGF-1R/PI3K. *Cancer Cell* **18**:683–695.

Address correspondence to: William F. Elmquist, Department of Pharmaceutics, University of Minnesota, 9-177 Weaver Densford Hall, 308 Harvard Street SE, Minneapolis, MN 55455. E-mail: elmqu011@umn.edu

Mechanisms Limiting Distribution of the BRAF^{V600E} Inhibitor Dabrafenib to the Brain: Implications for the Treatment of Melanoma Brain Metastases

Rajendar K Mittapalli, Shruthi Vaidhyanathan, Arkadiusz Z. Dudek, and William F. Elmquist

Journal of Pharmacology and Experimental Therapeutics

Supplemental Figure 1:

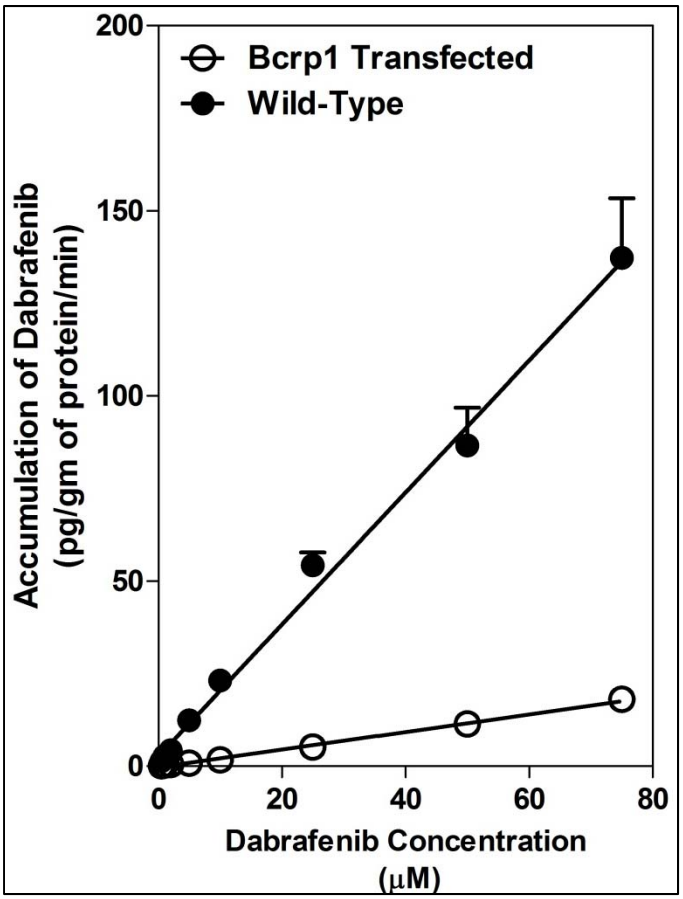

Figure Legend: Accumulation of different concentrations (0.5 to 75 μM) of dabrafenib in MDCKII- wild type and Bcrp1 transfected cell lines. The data show a linear correlation between concentration and cellular accumulation indicating no saturation of these active efflux transporters. Data represent Mean ± SD; n= 3 for all data sets.

Mechanisms Limiting Distribution of the BRAF^{V600E} Inhibitor Dabrafenib to the Brain: Implications for the Treatment of Melanoma Brain Metastases

Rajendar K Mittapalli, Shruthi Vaidhyanathan, Arkadiusz Z. Dudek, and William F. Elmquist

Journal of Pharmacology and Experimental Therapeutics

Supplemental Figure 2:

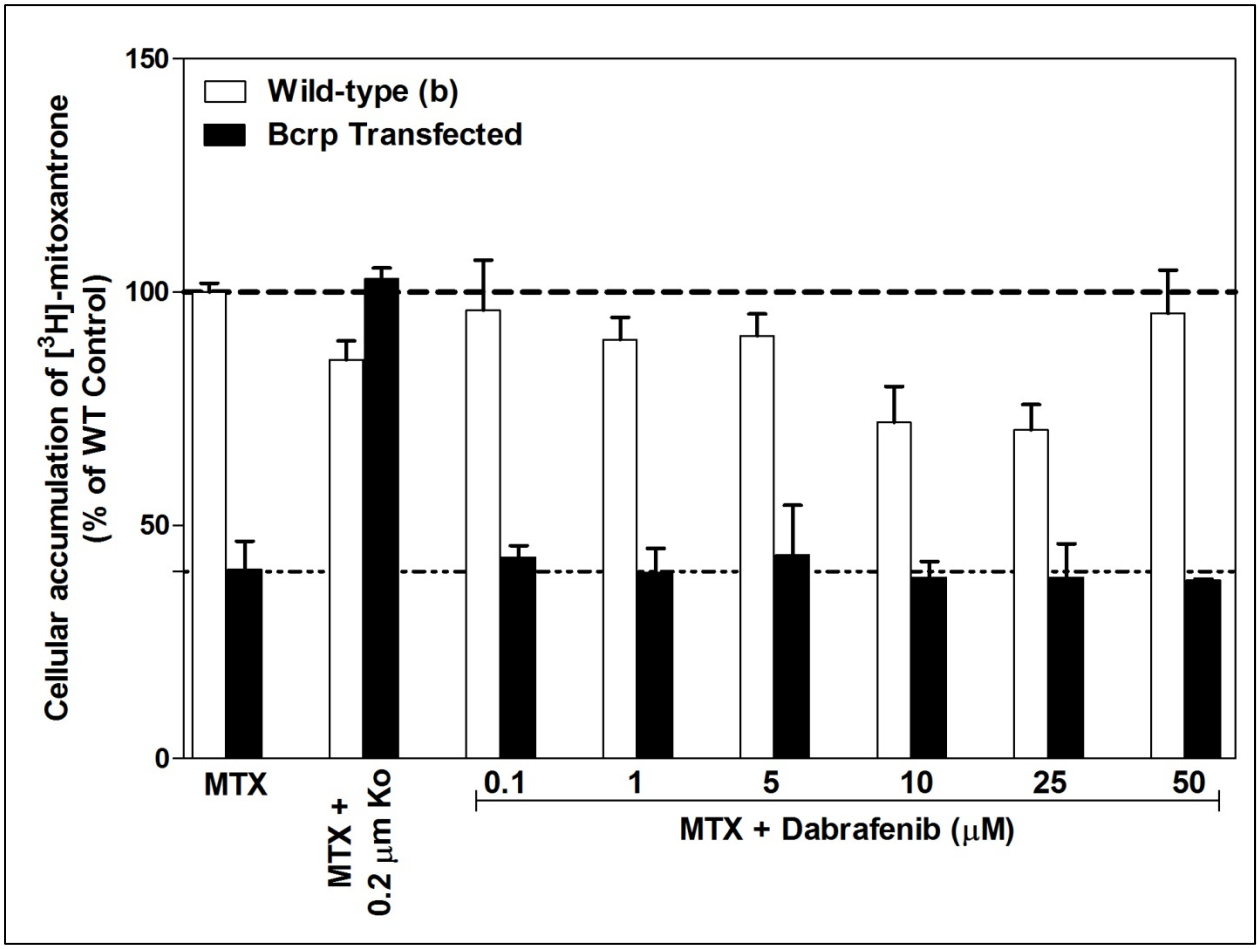

Figure Legend: Intracellular accumulation of [^{3}H]-mitoxantrone (MTX; Bcrp probe substrate) in Bcrp1-transfected cell lines with increasing concentrations of dabrafenib from 0.1 µM to 50 µM. Ko: Bcrp inhibitor Ko143; Data represent mean ± SD; n = 3 for all data points.

Mechanisms Limiting Distribution of the BRAF^{V600E} Inhibitor Dabrafenib to the Brain: Implications for the Treatment of Melanoma Brain Metastases

Rajendar K Mittapalli, Shruthi Vaidhyanathan, Arkadiusz Z. Dudek, and William F. Elmquist

Journal of Pharmacology and Experimental Therapeutics

Supplemental Figure 3:

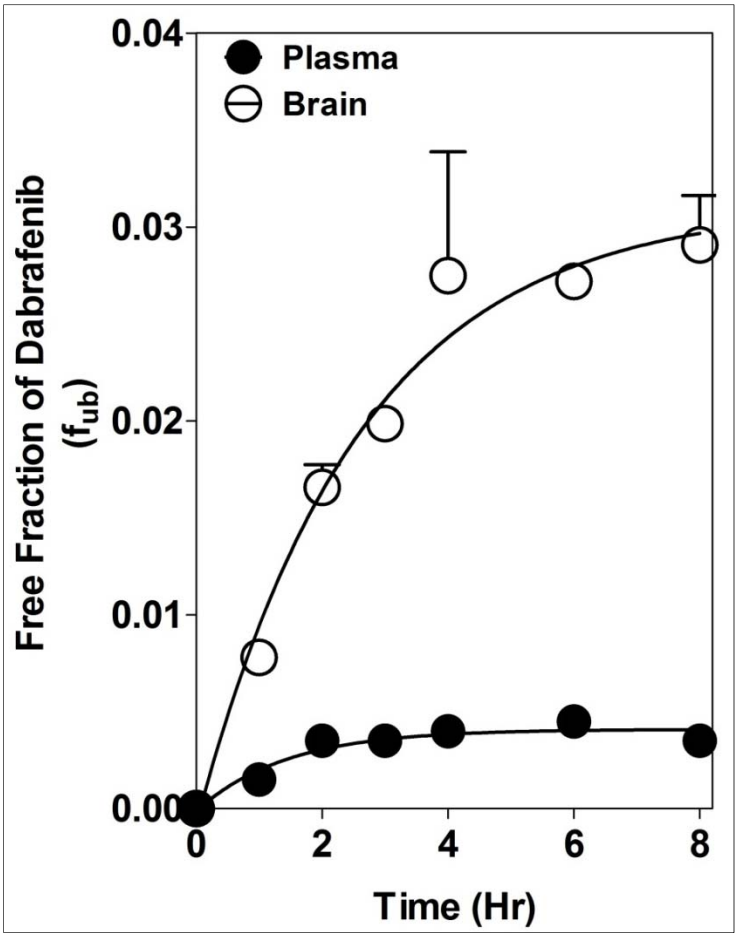

Figure Legend: Equilibrium dialysis in plasma and brain homogenate: The graph shows the free fraction of dabrafenib (fraction unbound, f_{ub}) in plasma and brain homogenate with respect to time. The data indicate that equilibrium is achieved in ~6hrs in both plasma and brain homogenate.